Supporting Information

Behera and Theil 10.1073/pnas.1318417111

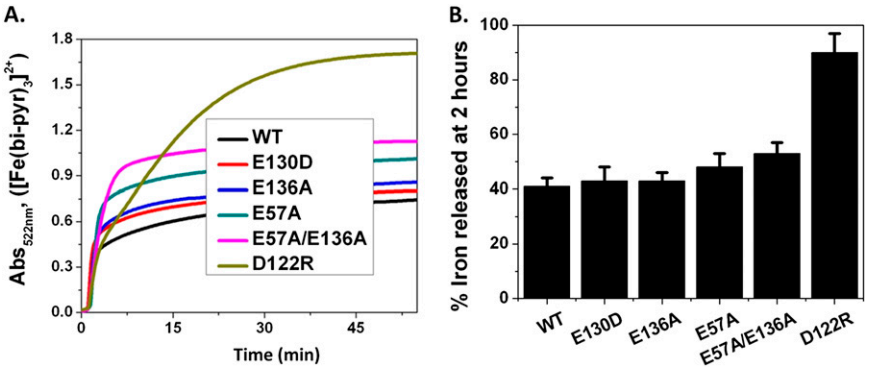

Fig. S1. Transfer site variants E57A and E136A and ion channel constriction variant E130D have very small effects on mineral dissolution and Fe exit contrasting with ion channel gating variant D122R. Mineral dissolution was analyzed in recombinant ferritin protein cages and mineralized by adding 480 Fe/cage and the release of Fe^{2+}-bipydridyl outside the cage after adding NADH+ FMN as the reductant. (*A*) Progress curve of Fe^{2+}-bipyridyl. (*B*) Percent total Fe released in 2 h. The gating variant D122R, part of the Q6, N7, R72, and D122 bonding network at the external channel gate (1), has released all of the iron by 2 h and indeed by 45 min (*A*), contrasting with WT and the midchannel constriction ferritin variant E130D and transfer site variants E57A, E136A, and E57A/E136A.

1. Tosha T, et al. (2012) Ferritin protein nanocage ion channels: Gating by N-terminal extensions. *J Biol Chem* 287(16):13016–13025.

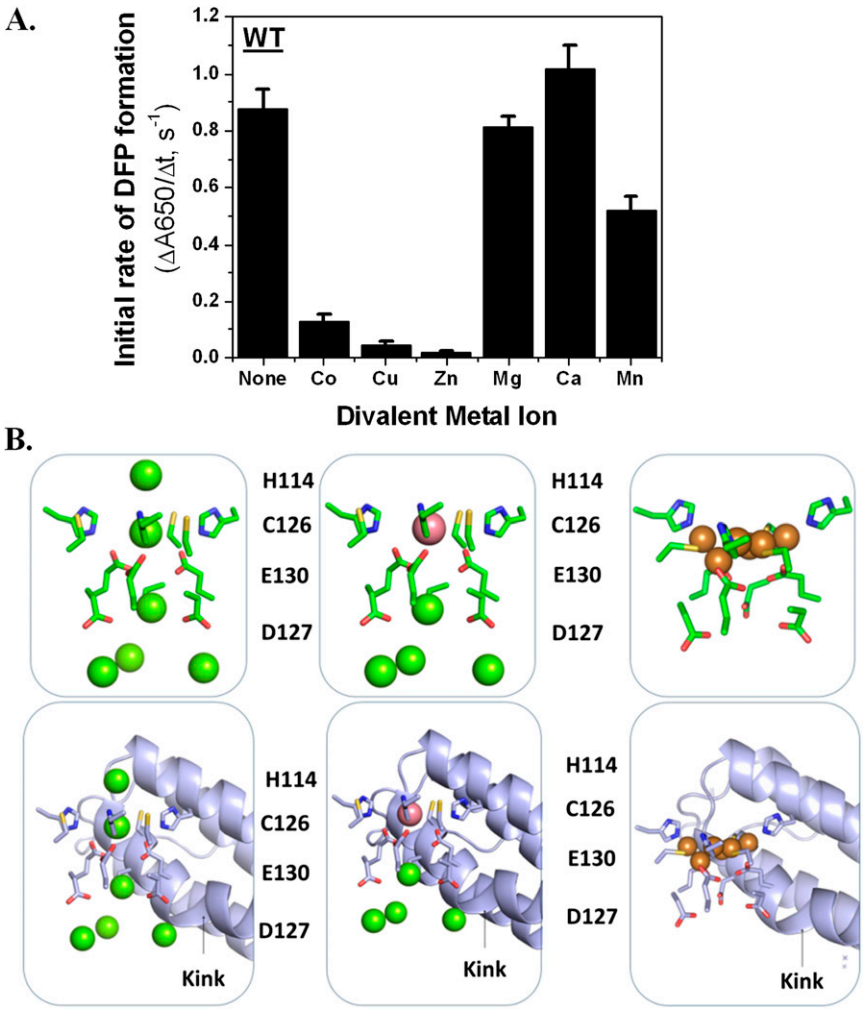

Fig. S2. Divalent metal ion inhibition of ferritin catalysis and binding sites in ferritin threefold ion channels. (*A*) Changes in the initial rates of DFP formation in WT ferritin (Table S5). (*B*) Divalent metal binding in the ion channels of ferritin protein cages. The channels are formed by residues from protein subunit helix 4 and H114 in helix 3. The position of Zn^{2+} ions and the conformation of C126 residues in the ferritin ion channels are identical to Cu^{2+} in ferritin protein structures. (*Left*) PDB file 3KA3 (Mg^{2+}), (*Center*) PDB 3KA4 (Co^{2+}), and (*Right*) PDB 3RE7 (Cu^{2+}), using PYMOL. Spheres: green, Mg^{2+}; pink, Co^{2+}; reddish-brown, Cu^{2+}.

Table S1. Metal ion binding sites in ferritin protein cages

Metal ion	Ferritin used for crystallization (PDB code)	In the threefold ion channel (*n*, number of metal ions)	Transfer sites	Redox sites (two metal ions)	Adjacent sites	Fourfold axes	Total no. metal/(channel + transfer + redox sites)	Ref(s).
				Protein crystals				
Mg^{2+}*	Frog M-ferritin (3KA3)	T118, E130, S131, D127; $n = 6$	E57, E136 ($n = 1$);	E23, E58, H61; Q137, D140, E103; $n = 2$	H54		48+24+48 = 120	(1, 2)
Fe^{3+}† (soak)	Frog M-ferritin (3RGD)	E130a,b,c; $n = 1$	n = 0	E23, E58, H61, E103, Q137; $n = 2$	H54	His169	8 + 0 + 48 = 56	(3)
Co^{2+}‡ and Mg^{2+}‡	Frog M-ferritin (3KA4)	E130a,b,c; $n = 1$	E57, E136; n = 1.0; E57; n = 15	E23, E58, H61; n = 1.0; E58, E103; n = 1.0	H54	His169	8+ 48+ 48 = 104; 302 with Mg^{2+}	(2)
Cu^{2+}§ (soak)	Frog M-ferritin (3RE7)	E130, H114, C126 ($n = 3$); E130, C126 ($n = 2$); C126, H114 ($n = 1$)	E57, E136 ($n = 1$)	E23, E58, H61, E103; $n = 2$	H54	His169	48+24+48 = 120	(3)
Ca^{2+}¶ and Zn^{2+}¶ (soak)	Human H-ferritin (2CEI)	E130, H114, C126 ($n = 3$); E130, C126 ($n = 3$); D127-H_2O ($n = 1$)	n = 0	E23, E58, H61, E103; $n = 2$	H54	His169	56+0+48 = 104	(4)
				VTHMCD/CD				
Fe^{2+}	Frog M-Ferritin	Not applicable	Not applicable	Fe1-23 (Bidentate), E58, H61, H_2O; Fe2- E58, E103, Q137, D140, H_2O	Not applicable	Not applicable	48 (Active site only)	(5)

*Cocrystalized with 2 M $MgCl_2$ in 100 mM BICINE (pH 9.0).
†Demineralized ferritin crystallized from 20 mM Tris·HCl (pH 7.5) and 2.1 M sodium formate and later soaked in 64 mM $FeSO_4$ $7H_2O$ (~24Fe/subunit).
‡Cocrystallized with 100 mM $CoCl_2$ and 2 M $MgCl_2$ in 100 mM BICINE (pH 9.0).
§Crystallized from 20 mM Tris·HCl (pH 7.4) and 2.5 M sodium formate and later soaked with 20 mM $CuSO_4{\cdot}5H_2O$ solution (~16Cu/subunit).
¶Crystallized from 50 mM Hepes (pH 7.5) and 5.7 mM $CaCl_2$ and later soaked with 10mM $ZnCl_2$.

1. Tosha T, et al. (2012) Ferritin protein nanocage ion channels: Gating by N-terminal extensions. *J Biol Chem* 287(16):13016–13025.
2. Tosha T, Ng HL, Bhattasali O, Alber T, Theil EC (2010) Moving metal ions through ferritin-protein nanocages from three-fold pores to catalytic sites. *J Am Chem Soc* 132(41):14562–14569.
3. Bertini I, et al. (2012) Structural insights into the ferroxidase site of ferritins from higher eukaryotes. *J Am Chem Soc* 134(14):6169–6176.
4. Toussaint L, Bertrand L, Hue L, Crichton RR, Declercq JP (2007) High-resolution X-ray structures of human apoferritin H-chain mutants correlated with their activity and metal-binding sites. *J Mol Biol* 365(2):440–452.
5. Schwartz JK, Liu XS, Tosha T, Theil EC, Solomon EI (2008) Spectroscopic definition of the ferroxidase site in M ferritin: Comparison of binuclear substrate vs cofactor active sites. *J Am Chem Soc* 130(29):9441–9450.

Table S2. Amino acid substitution of conserved ion channel or intrasubunit transfer residues alters DFP and Fe^{3+}–O kinetics in ferritin

Protein	$\Delta A_{650\ nm}$/s, DFP, 96 Fe^{2+}/cage	V_{max}- ($\Delta A_{650\ nm}$/s), DFP	k_{cat} (s^{-1}), DFP, 650 nm	K_m/site (μM), DFP, 650 nm	k_{cat}/K_m ($s^{-1}\mu M^{-1}$), DFP, 650 nm	Hill coeff. (n)	Saturating Fe^{2+}/cage	V_{max}* ($\Delta A_{350\ nm}$/s), $Fe^{3+}O$ species
WT	1.18 ± 0.12	2.70 ± 0.13	108 ± 5	5.4 ± 0.6	20.0 ± 2.1	1.6 ± 0.1	197 ± 10	3.30 ± 0.2
				Transfer residues				
E136A	0.37 ± 0.02	2.01 ± 0.12	80 ± 5	13 ± 1	6.4 ± 0.6	1.6 ± 0.2	435 ± 20	2.82 ± 0.09
E57A	0.25 ± 0.05	2.40 ± 0.15	96 ± 6	15 ± 2	6.5 ± 0.8	1.5 ± 0.1	550 ± 24	3.20 ± 0.15
E57A/E136A	0.04 ± 0.02	0.81 ± 0.02	32 ± 1	27 ± 2	1.2 ± 0.1	1.6 ± 0.1	1180 ± 29	1.53 ± 0.08
				Channel residues				
E130D	0.24 ± 0.02	1.40 ± 0.05	56 ± 2	7.9 ± 0.5	7.1 ± 0.5	2.0 ± 0.2	390 ± 15	1.70 ± 0.10
E130A	0.002 ± 0.001	N. D	N. D	N. D	—	—	—	—
D127A	0.013 ± 0.002	—	—	—	—	—	>3300	—

The $2Fe^{2+}/O_2$ redox catalysis was initiated by rapid mixing and monitored as diferric peroxo (DFP, λ_{max} = 650 nm) intermediates (1 catalytic center/subunit; 24/cage) (1). k_{cat} was estimated from DFP: ε = 1,000 $M^{-1}\cdot cm^{-1}$) (2). K_m/site was computed as [Fe]/24; 24, number of catalytic site/protein cage. Cooperativity, $V_i = V_{max}[Fe^{2+}]^n/((K_m)^n + [Fe^{2+}]^n)$ obtained from plots of V_i vs. $[Fe^{2+}]$, Hill coefficient (n) values are significantly ($P < 0.001$) >1.0. The data are averages of three to four independent experiments, using two different protein preparations of each protein with the error as SD. Final concentrations of ferritin protein cages were 1.04 μM in 0.1M Mops·Na, pH 7.0, 0.1 M NaCl.

*Absorbance at 350 nm in the center of the broad transition, 300–500 nm of $Fe^{3+}O$ species (DFP and diferric oxo and $Fe^{3+}O$ nuclei and $Fe_2O_3{\cdot}H_2O$ mineral).

1. Liu X, Theil EC (2004) Ferritin reactions: Direct identification of the site for the diferric peroxide reaction intermediate. *Proc Natl Acad Sci USA* 101(23):8557–8562.
2. Pereira AS, et al. (1998) Direct spectroscopic and kinetic evidence for the involvement of a peroxodiferric intermediate during the ferroxidase reaction in fast ferritin mineralization. *Biochemistry* 37(28):9871–9876.

Table S3. Substitution at conserved negatively charged residues alters $2Fe^{2+}/O_2$ enzymatic reactions in ferritin for single turnover (formation and decay) of DFP and Fe^{3+}–O

Protein	Initial rate of DFP formation ($\Delta A650/\Delta t$), s^{-1}	DFP decay rate constant (A650), s^{-1}	Initial rate of Fe^{3+}–O formation ($\Delta A350/\Delta t$), s^{-1}	A350 at 5 s
WT	0.99 ± 0.06	1.56 ± 0.07	1.30 ± 0.10	0.16 ± 0.01
E130D	0.45 ± 0.03*	1.48 ± 0.02		
E60A	1.04 ± 0.08 N.S.	1.23 ± 0.02*	1.40 ± 0.02 N.S.	0.18 ± 0.01 N.S.
E136A	0.68 ± 0.01*	1.09 ± 0.02*	1.14 ± 0.03***	0.19 ± 0.01•
E57A	0.33 ± 0.03*, **	1.28 ± 0.03*, **	0.71 ± 0.06*, **	0.21 ± 0.03•, ••
E157A/E136A	0.069 ± 0.005*, **	0.66 ± 0.08*, **	0.14 ± 0.01*, **	0.16 ± 0.01 N.S.
D127A	0.015 ± 0.007*, **	0.39 ± 0.09*, **	0.04 ± 0.01*, **	0.10 ± 0.01*, **
D127A/E136A	0.008 ± 0.003*, N.S.	0.32 ± 0.04*, N.S.	0.03 ± 0.01*, N.S.	0.09 ± 0.01*, ••
D127A/E57A	0.005 ± 0.002*, **	0.15 ± 0.03*, **	0.02 ± 0.01*, N.S.	0.13 ± 0.02***, **

The $2Fe^{2+}/O_2$ reactions were initiated by rapid mixing (<5 ms) equal volumes of solutions of 200 μM solutions of $FeS0_4$ in 1 mM HCl and 4.16 μM solutions of M ferritin protein cages (100 μM subunits), in 0.2 M Mops, 0.2 M NaCl, pH 7.0. Initial rates of formation of DFP (λ_{max}, 650 nm) and Fe^{3+}–O mixture, measured at 350 nm, were calculated by fitting the linear part (6–35 ms) of each kinetic trace (Fig. 2) except D127A, D127A/E136A, and D127A/E57A, where the time range used was 10–100 ms. DFP decay rate constants were computed by fitting the decay part of A650 time courses (Fig. 2) to the first exponential equation for all of the proteins. Data are the mean ± SD of four to eight independent experiments, using two to five different protein preparations of each protein. Compared with WT: **$P < 0.05$, ***$P < 0.001$, *$P < 0.0001$; N.S., no significant difference; E136A, E57A/E136A compared with E57A or D127A compared with D127A/E136A and D127A/E136A.

Table S4. Ferritin transfer residue variants resist Fe^{2+}-enhanced catalytic turnover

	DFP decay rate constant, s^{-1}	
Protein	k_{48}, 48 Fe/cage	k_{480}, 480 Fe/cage
WT	1.56 ± 0.07	5.33 ± 0.27*
Ion channel residues		
E130D	1.48 ± 0.02	4.7 ± 0.20
D127A	0.39 ± 0.09*, **	1.30 ± 0.01*, **
Transfer residues		
E136A	1.09 ± 0.02*	1.93 ± 0.23*
E57A	1.28 ± 0.03*, **	2.05 ± 0.04*, N.S.
E157A/E136A	0.66 ± 0.08*, **	1.22 ± 0.01*, **

	DFP half-life ($t_{1/2}$), s		
Protein	48 Fe^{2+}/cage	480 Fe^{2+}/cage	Ratio $t_{1/2}$ (48 Fe/480 Fe)
WT	0.44 ± 0.02	0.13 ± 0.01	3.42 ± 0.25
Ion channel residues			
E130D	0.47 ± 0.02	0.15 ± 0.02	3.23 ± 0.20
D127A	1.78 ± 0.17*, **	0.53 ± 0.02*, **	3.33 ± 0.05
Transfer residues			
E136A	0.64 ± 0.01*	0.36 ± 0.04*	1.77 ± 0.30
E57A	0.54 ± 0.02*, **	0.34 ± 0.02*, N.S.	1.60 ± 0.04
E157A/E136A	1.05 ± 0.09*, **	0.57 ± 0.02*, **	1.85 ± 0.03

The DFP decay rate constants were computed by fitting the decay part of $A_{650\ nm}$ progress curves to the first exponential equation for all of the proteins. *$P < 0.0001$, significantly different, compared with WT (*t* test); **$P < 0.001$, significantly different; N.S., not significantly different ($P > 0.05$). The *P* values for DFP decay rate constants were computed for E57A against E136A, E57A/E136A, and D127A against E57A.

Table S5. Divalent metal ions (M^{2+}) selectively inhibit DFP formation

Protein	Initial rate of DFP formation (ΔA650/Δt), s^{-1}	Inhibition
WT ferritin	0.89 ± 0.06	1.0
WT ferritin + Mg^{2+}	0.81 ± 0.04	1.1
WT ferritin + Ca^{2+}	1.02 ± 0.08	0.9
WT ferritin + Mn^{2+}	0.52 ± 0.05	1.7
WT ferritin + Co^{2+}	0.13 ± 0.02	6.8
WT ferritin + Cu^{2+}	0.04 ± 0.01	22.2
WT ferritin + Zn^{2+}	0.01 ± 0.01	89.0

A control reaction does not incubate with M^{2+} ion; 4.16 μM ferritin was premixed with 48 M^{2+}/nanocage and incubated at room temperature for 1 h. The kinetics of the reactions (48 Fe/cage) were initiated by mixing preincubated ferritin nanocage and freshly prepared 200 μM ferrous sulfate solutions using the stopped flow instrument. The ratio of M^{2+} to Fe^{2+} was maintained 1:1. The final concentration of buffer in the solution was 0.1 M Mops, 0.1 M NaCl, pH 7.0. Initial rates of formation of DFP at 650 nm were calculated by linear fitting the rising part of each kinetic trace for all of the proteins. Note that the data shown are averages (±SD) of two to four independent experiments, using one to three different protein preparations of each protein.